A Defect-Free Principle for Advanced Graphene Cathode of Aluminum-Ion Battery

*Hao Chen, Fan Guo, Yingjun Liu, Tieqi Huang, Bingna Zheng, Nimrodh Ananth, Zhen Xu, Weiwei Gao, and Chao Gao**

Advanced energy storage systems with high energy density, power density, and safety have long been the subject of concentrated studies to meet the ever-growing demand of numerous electric devices.[1–3] In this regard, rechargeable aluminum-based battery is of particular attraction since it can offer considerable advantages of high anode capacity, safety and cost-effectiveness, due to the low-cost and incombustible nature of aluminum (Al) metal anode with ultrahigh theory capacity of 2978 mAh g^{-1} and 8034 mAh L^{-1}. However, the major challenge for aluminum-ion battery (AlB) resides in cathode material, which only exhibited low discharge potential (<1.2 V), low current density (<1 A g^{-1}) and short cycle life (<100 cycles) in previous reports.[4–8] This leads to researches in AlB over past 30 years hard to compete with those of other battery systems. Recently, Dai et al. made a breakthrough in AlB using an ionic liquid electrolyte and graphitic foam cathode, which dramatically improve the performances of cathode material with high discharge voltage (1.8 V), stable specific capacity (60 mAh g^{-1}), long cycle life (7500 cycles), and high-rate performance (6 A g^{-1}).[9–11] Despite these efforts, there remain two key challenges facing AlB cathode: the low capacity limits the cell energy density, and insufficient high-rate performance causes cell power density inferior to supercapacitors.

Here we propose a defect-free principle to design graphene-based cathode. We first produced a cathode of highly crystallized defect-free few-layer graphene aerogel (GA),[12] paired with an anode of Al foil to bring about a highly performed Al–graphene battery (Al–GB). This novel defect-free design results in completely crystallized sp^2 carbons in GA's atomic structure, which has three notable advantages: (1) elimination of inactive defects facilitating the fast intercalation of large-sized anions[13] and simultaneously providing more active sites for energy storage; (2) greatly enhanced electrical conductivity recovering defective graphene into electrical highway;[14] and (3) high reproducibility of material quality and cell performance favoring large-scale manufacture. Owing to these merits, the defect-free GA cathode set new records for the performances of AlB cathode (e.g., 100 mAh g^{-1} at 5 A g^{-1} with average discharge point at 1.95 V, 97% capacity retention after 25 000 cycles, 97 mAh g^{-1} at 50 A g^{-1}). Significantly, the defect-free principle is generally appropriate to design graphene-based electrodes of other battery systems.

Scalable manufacture with good reproducibility is of importance for practical applications of batteries. To this end, we set up a simple, highly controllable, and scalable approach to fabrication of graphene cathode using commercial materials and industrially viable production equipments (**Figure 1**a–c). We select graphene oxide[15–18] (GO, average lateral size of 50 μm) as the raw material for its ton-level mass productivity. However, GO has numerous defects and oxygen-containing groups that negatively affect electrochemcial property. Accordingly, we employ a well-established high-temperature annealing technology to restore those defects, achieving high-quality defect-free graphene.[19,20] GA is selected as the cathode material for its porous yet continuous structure. The porosity has two main roles: facilitating electrolyte immersion and avoiding over-stacking of graphene during graphitization. Meanwhile the continuous graphene network benefits electron transportation and high-rate performance.

Graphene cathode was made by three steps: (i) preparation of reduced GO aerogel[12,21,22] (rGA) via a reported freeze-dry method followed by chemical reduction;[23] (ii) thermal annealing of rGA to achieve GA; and (iii) mechanical compression of GA to get the target cathode paper. The brown rGA transformed into silver black GA as annealed at 3000 °C (GA-3000, Figure 1d). The compressed, silver glitter cathode papers or strips (density of 0.5 g cm^{-3}) exhibit outstanding flexibility, foldability, and twistability (Figure 1e–g; Figure S1, Supporting Information).[24] Likewise, we also fabricated GA-2000 and GA-2500 annealed at 2000 and 2500 °C, respectively (Figure 1a,b; Figure S2, Supporting Information).[20,25] Compared with other techniques to enhance the performance of graphene electrode, such as heteroatom doping and chemical vapor deposition, our methodology has distinguished advantages: easy control over material uniformity at both local structures of graphene and different batches of product owing to no uncertain doping sites and amounts, highly electrical conductivity due to the recovery of perfect graphene structures, and scalable productivity because of the simple fabrication process, large availability of raw materials and apparatuses, and high repeatability.[26] The detailed experiments are elucidated in the Supporting Information.

No obvious change was found in microsized structure of GA during the annealing process from the typical scanning electron microscopy (SEM) images (Figure S2, Supporting Information), indicating the remaining of graphene sheet morphology in an ultrahigh temperature inert atmosphere.

H. Chen, F. Guo, Y. Liu, T. Huang, Dr. B. Zheng, Dr. N. Ananth, Dr. Z. Xu, Dr. W. Gao, Prof. C. Gao
MOE Key Laboratory of Macromolecular Synthesis and Functionalization
Department of Polymer Science and Engineering
Key Laboratory of Adsorption and Separation Materials and Technologies of Zhejiang Province
Zhejiang University
38 Zheda Road, Hangzhou 310027, P. R. China
E-mail: chaogao@zju.edu.cn

DOI: 10.1002/adma.201605958

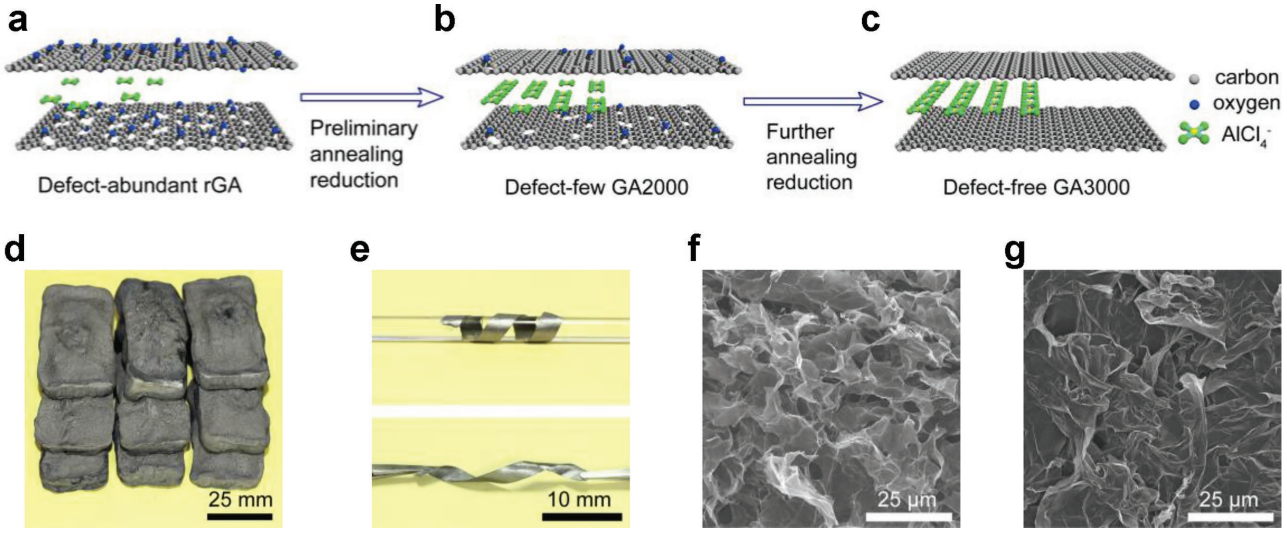

Figure 1. Design and production of GA cathode. a–c) Schematic of the defect-free design. Defects (sp^3 carbons and oxygen-containing groups) in a) rGA and b) GA-2000 reduce the electrical conductivity, impede the transportation of $AlCl_4^-$ and cannot act as active sites; c) the defect-free sp^2 carbon networks in GA-3000 act as active sites and facilitate the transportation of $AlCl_4^-$. d) Digital camera image of GA-3000. e) A compressed GA-3000 strip is coiled around a glass rod to illustrate the good flexibility and twisted by two tweezers to show the twistability. f,g) SEM images of f) GA-3000 and g) compressed GA-3000 paper.

The atomic-scale structure displayed great evolution identified by the high-resolution transmission electron microscopy (HRTEM). Preliminary annealing at 2000 °C enabled small part of defect configurations to relax to sp^2 carbons in atomic-scale structure, and GA-2000 still exhibited abundant vacancy holes and disordered carbon network (**Figure 2**a). Annealing at 2500 °C further restored most of hexagonal 2D lattice, and a few random patches of polygons and atomic vacancy holes were still observed in GA-2500, impeding the formation of long-range crystalline order along the zig-zag and armchair chains (Figure 2b). These vacancy holes and polygons are visual sites of disordered defects.[27] Annealing at 3000 °C completely healed the defect configurations of chemically converted graphene (CCG) to generate planar honeycomb crystal lattice, displaying

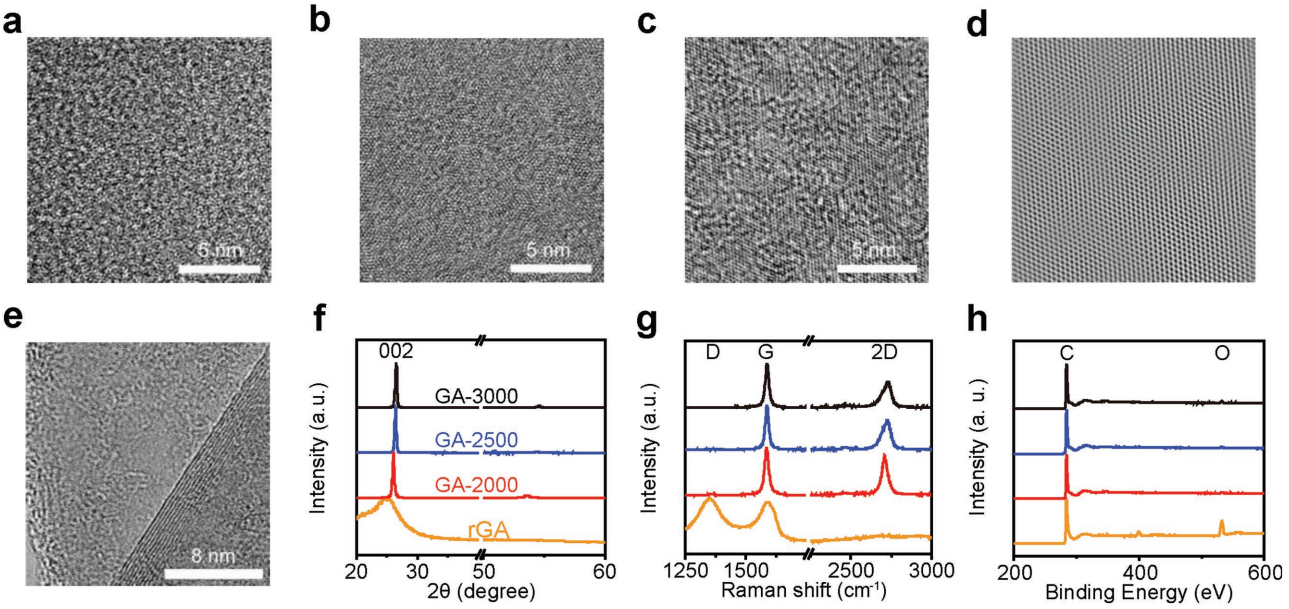

Figure 2. Structural characterizations of GAs. a–e) HRTEM images of a) GA-2000, b) GA-2500, c) GA-3000, and d) IFFT of GA-3000 showing the enhanced crystallinity of graphene with higher temperature annealing and e) stacked 4–10 graphene layers. f) X-ray diffraction (XRD) pattern of different GAs, a sharp (002) peak at $2\theta = 26.52°$ (d spacing = 0.335 nm) and a weak (004) peak at ≈54° of GA-3000 with neglectable change in the stacked structure between GA-2000, GA-2500, and GA-3000. g) Raman and h) XPS spectra illustrating the evolution of different GAs. In XPS spectra, the oxygen concentration decreased from 11.82% (rGA), 5.57% (GA-2000), 5.01% (GA-2500) to 1.84% (GA-3000), the oxygen-concentration in GA-3000 was almost neglectable due to the absorbance of oxygen on the graphene surface.

long-range crystalline arrangement of sp^2-bonded carbon hexagons and large-sized sp^2 domains without any detectable defect sites (Figure 2c; Figure S3, Supporting Information).[20,25] Such a gradual high-temperature annealing process to amend the defects of CCG reminds us of realistic road construction and repairing: from a wetland with abundant traps (Figure 1a, rGA) to a bumpy road with many traps (Figure 1b, GA-2000), and eventually to a trap-free smooth highway (Figure 1c, GA-3000). Inverse fast Fourier transform (IFFT) was conducted to obtain an atomic-resolved lattice image (Figure 2d) by masking the sixfold symmetry characteristic diffraction spots of GA-3000 in fast Fourier transform image (Figure S3, Supporting Information). The large-area, perfect 2D lattices with continuous zigzag chain and armchair chain[27] in both HRTEM and IFFT images demonstrate highly crystallized, defect free graphene indeed in GA-3000. In addition, slightly stacked few-layer graphene sheets (4–10 layers; Figure 2e) in GA-3000 were observed in HRTEM images, successfully prevented it from graphite-like severe stacking by the porous aerogel structure.

The gradual decline of defects is supported by Raman spectroscopy and X-ray photoelectron spectroscopy (XPS). As shown in Figure 2g, the intensity ratio of D band (at ≈1350 cm^{-1}, resulted from the disordered defect-induced double-resonant Raman process[28]) to G band (at ≈1598 cm^{-1}, for in-plane vibration of highly symmetrical sp^2 carbon hexagonal) decreased from 1.3 (rGA) to 0.039 (GA-2000), then to 0.01 (GA-2500) and almost 0 (GA-3000). The I_D/I_G value of GA-3000 is obviously lower than those of natural graphite (0.0359–0.0721) and graphene grown by chemical vapor deposition (≈0.125)[29–31] which are widely recognized as high-quality graphene sources. The decline of D band intensity consolidates that the defects gradually diminished during the high-temperature annealing to access defect-free graphene,[32] substantially consistent with the decline of oxygen concentration illustrated in XPS spectra (Figure 2h) and defects' gradual vanishment in the above HRTEM images (Figure 2a–c).

The favorable effects of defect-free design on GA cathodes were verified by cyclic voltammetry (CV) and galvanostatic cycling tests in coin cells. Three anodic peaks at 2.0, 2.3, and 2.42 V are observed in the CV curves due to the intercalation of $AlCl_4^-$ into graphene of different stages. Correspondingly, two cathodic peaks are found at 1.8 and 2.22 V attributed to the deintercalation of $AlCl_4^-$ (Figure S4, Supporting Information). When the graphene cathode was removed from the battery, these peaks disappeared, manifesting that the redox reactions were carried in the graphene material (Figures S5–S7, Supporting Information).

Figure 3a shows the long-term galvanostatic cycling of GA-3000 cathode. It exhibits a high and stable specific discharge capacity of 100 ± 3 mAh g^{-1} after a few cycles of activation at a current density of 5 A g^{-1} (50 C, charge/discharge in 72 s). Surprisingly, this cathode affords a superb capacity retention with 97% of the highest capacity after 25 000 cycles and a Coulombic efficiency higher than 98%. Discharge curves over 25 000 cycles show two discharge voltage plateaus at ≈2.3 V (0–30 mAh g^{-1}) and ≈1.8 V (50–90 mAh g^{-1}), in accordance with the cathodic peaks in CV curves. The charge/discharge curves retained well during the ultralong cycling with few declines of the initial charging voltage, declaring the excellent electrochemical stability of the GA-3000 cathode (Figure 3b). Given both parameters of high-specific capacity and high Coulombic efficiency, 2.51 V was the ideal cutoff voltage for GA-3000 cathode (Figure 3c; Figure S7, Supporting Information).

Meanwhile, overlapped discharge curves and close capacities of ≈100 mAh g^{-1} were performed at different rates from 2 C to 50 C while charging at 50 C (Figure 3d; Figure S8, Supporting Information). Importantly, at higher rates from 100 C to 500 C, the charging and discharging capacities impressively retained ≈100 mAh g^{-1} (97 mAh g^{-1} at 500 C) with slightly decline of the average discharge voltage (**Table 1**) and increment of overpotential (Figure 3e). Notably, at an ultrahigh current density of 100 A g^{-1} (1000 C), a capacity of 74 mAh g^{-1} with average discharge voltage of 1.3 V was attained (charging and discharging in 2.7 s; Figure S9, Supporting Information). The two discharging voltage plateaus aforementioned are still recognized easily despite the high current density is up to 500 C (charging and discharging in 7.2 s). The high-rate performance benefits from efficient kinetic reaction process with a small barrier attributed to fast electron transportation[14] (Table S2, Supporting Information) and fast intercalation of $AlCl_4^-$ into defect-free graphene layers.[33,37] All these performances: high specific capacity, high discharge voltage, excellent cycle stability, and ultrahigh rate performance far surpass those of the previously reported Al–carbon batteries (Figure 3f). Furthermore, more than 100 pieces of GA-3000 cathode have been tested, and all of them delivered stable specific capacity higher than 97 mAh g^{-1} (Figure S9c, Supporting Information), demonstrating the excellent reproducibility in both material quality and electrochemical property due to the defect-free design. This is essentially different from the previous methodologies such as heteroatom doping[34] in which doping sites and concentrations are hard to be precisely controlled, especially in the case of large-scale production.[35]

To reveal the advantages of defect-free graphene cathode, we also prepared controlled samples of GAs annealed at 2000 and 2500 °C. Figure 3g and Table 1 compare the performances of GAs with controlled concentration of defects. Basically, GA-2000 cathode showed lower capacity (45 mAh g^{-1} at 50 C) and worse high-rate performance (Figure S10, Supporting Information) than GA-2500 cathode (80 mAh g^{-1} at 50 C), and their performances cannot compete with those of GA-3000 cathode. The charge/discharge curves suggest that the higher annealing temperature employed, the higher average discharge voltage and lower overpotential exhibited (Table 1; Figures S10 and S11, Supporting Information). Comparisons of these electrochemical performances of different GA cathodes strongly support that the more defects exist, the worse the performances are.

To substantiate the negative effects of defects, in situ and ex situ Raman spectra were performed on a defective GA-2000 cathode, probing the possible interaction of $AlCl_4^-$ with highly crystallized sp^2 carbon and defects during charging/discharging process (**Figure 4**a,b). The G band of GA-2000 cathode blueshifted from 1591 to 1623 cm^{-1}, further to doublet peak at 1624 and 1639 cm^{-1} and eventually to 1639 cm^{-1} during the charging process in Figure 4a. These large upshifts of 48 cm^{-1} demonstrate that it is $AlCl_4^-$ ion that intercalates into graphene layers instead of Cl^- ion,[36,37] which was consistent with the calcination test reported before.[9] Reverse redshifts were

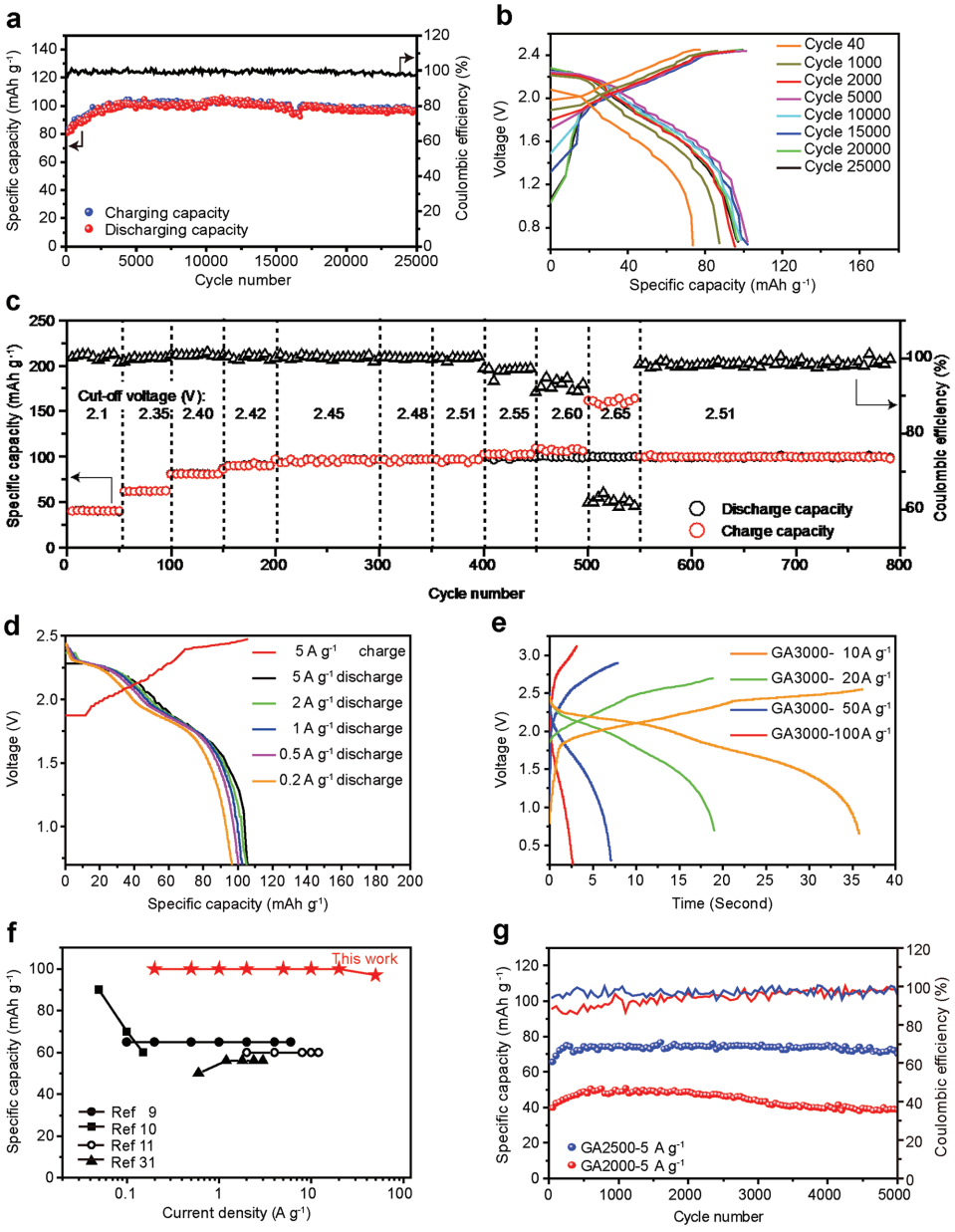

Figure 3. a) Galvanostatic cycling of GA-3000 (5 A g^{-1}) over 25 000 cycles. b) Detailed charge and discharge curves of GA-3000 cathode at different cycles (50 C). c) The specific capacity and Coulombic efficiency of GA-3000 cathode at different cutoff voltage. Detailed data are listed in Table S1 in the Supporting Information. d) Charge and discharge profiles of GA-3000 cathode charged at 50 C and discharged at lower current densities. e) Charge and discharge curves of GA-3000 at higher current densities (from 100 C to 1000 C), the overpotential was calculated from the difference between the average charge voltage and average discharge voltage: 0.447 V for 100 C, 0.637 V for 200 C, and 1.09 V for 500 C. f) Comparison of specific capacity and rate performances of this work (GA-3000) with previously reported best values. g) Galvanostatic cycling of GA-2000 and GA-2500 at 5 A g^{-1}. 1 C = 100 mA g^{-1}.

correspondingly observed during the discharging process. These shifts provide a strong evidence for that, the highly crystallized sp^2 carbon regions enable the reversible storage of $AlCl_4^-$ ions by intercalation/de-intercalation. The intercalation causes charge transfer, intercalate-coupling and change of lattice constant during charging process, leading to blueshifts of G peak in Raman spectra.[38] On the contrast, the D band of the charged GA-2000 cathode, corresponding to the defects, delivered no shift compared with the discharged state. This demonstrated that the $AlCl_4^-$ anions did not intercalate into the defect sites. So defects, just like traps in a road, cannot act as active sites for $AlCl_4^-$ intercalation or enable the storage of $AlCl_4$ at all (Figure S12, Supporting Information). More clearly, the D band in ex situ Raman spectra showed no shift at all even if the cathode is charged (Figure 4b).[39] The 2D peak gradually disappeared during the intercalation and reappeared during the deintercalation, which is explained by the reversible coupling/decoupling between graphene layers in charging/discharging cycles.[40]

Table 1. Performances of different graphene aerogel cathodes.

Rate	GA-2000		GA-2500		GA-3000	
[C]	Specific capacity [mAh g^{-1}]	Average discharge voltage [V]	Specific capacity [mAh g^{-1}]	Average discharge voltage [V]	Specific capacity [mAh g^{-1}]	Average discharge voltage [V]
10	60	1.78	63–57	1.8	95 [5 C, 10 C, and 20 C]	1.94
30	52	1.69	80	1.85	100	1.95
50	45	1.68	80	1.85	100	1.95
100			75	1.626	100	1.846
200			61	1.37	97	1.727
500			47	1.2	97	1.55
Overpotential at 50 C [V]	0.77		0.4		0.29	

To prove the defect-free principle reversely, we study the possible reactions by setting a higher charge cutoff voltage that would fastly decompose the electrolytes and electrodes in conventional lithium battery systems[41] When the charge cutoff voltage was set at 2.55 V for GA-3000 at 50 C, the Coulombic efficiency gradually decreased from 95% to 30% after hundreds of cycles as shown in Figure 4c, resulting from the side reactions involving electrolyte decomposition[42] (Figures S6 and S7, Supporting Information). The specific capacity of GA-3000 cathode also gradually decreased from 100 to 70 mAh g^{-1} and cannot recover to 100 mAh g^{-1}, despite the cell was dissembled and the decayed cathode was reassembled with fresh counter electrode, separator and electrolyte (Figure 4c). These facts suggest that structure decomposition in GA-3000 causes the decline of cathodic capacity. The Raman spectra analysis of degraded GA-3000 at charge cutoff voltage of 2.55 V in Figure 4d reveals that the D band increased as the capacity faded, while the stable cathode at charge cutoff voltage of 2.51 V showed no emergence of D band after thousands of cycles as demonstrated in Figure 4e. HRTEM image of highly decayed GA-3000 cathode in Figure 4f shows that both sp^2 carbon hexagons and defects existed in the same graphene layer, dividing into sp^2 region full of hexagons and defect region mostly composed of polygons and vacancy holes. Notably, there are still some isolated

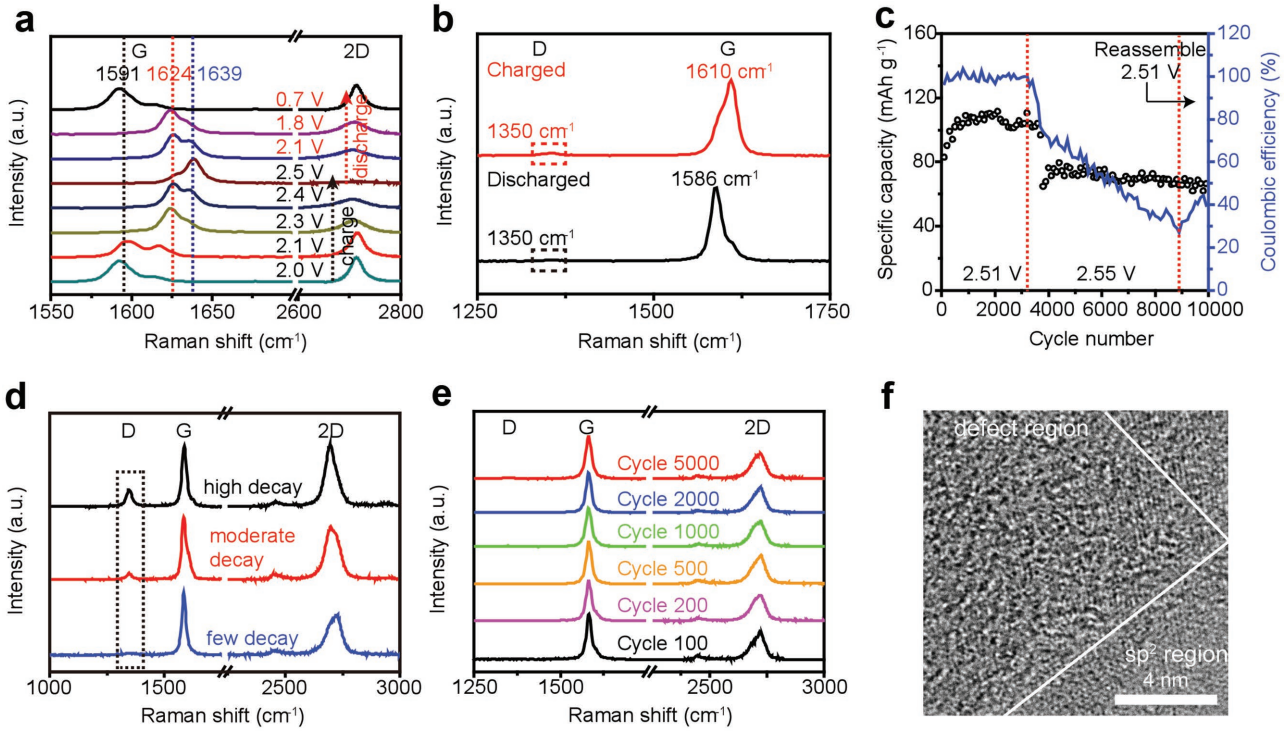

Figure 4. Evidence for defect-free principle. a) In situ and b) ex situ Raman spectra of GA-2000 during the charging and discharging process. c) Galvanostatic cycling of GA-3000 at charge cutoff voltages of 2.51, 2.55, and 2.51 V again for the reassembled cell. d) Raman spectra of decayed GA-3000 cathode at charge cutoff voltages of 2.55 V after different cycles (few decay: ≈80 mAh g^{-1} remained; moderate decay: 60 mAh g^{-1} remained; high decay: 20 mAh g^{-1} remained). e) Raman spectra of stable GA-3000 cathode at charge cutoff voltages of 2.51 V after different cycles. f) HRTEM image of highly decayed GA-3000 cathode.

yet aligned sp^2 carbon hexagons survived in the defect region, indicating that the defects were converted from the original sp^2 carbon[43] The XPS results of the decayed GA-3000 cathode indicate dramatical increase of the oxygen concentration (23.93%) and intensity corresponding to C—O—C in the deconvoluted C 1s spectra (Figures S13 and S14, Supporting Information). These Raman spectra, HRTEM images and XPS results were consistent with each other proving that defects were generated in GA-3000 cathode at a destructive charging cutoff voltage, which decayed the electrochemical performance.

For parallel demonstration of defect-free principle, other highly defective carbon materials (e.g., carbon fiber, rGA, and carbon black) were also used as cathodes for AlB. These materials all delivered neglectable capacity (<5 mAh g^{-1}) even at a low current density of 0.5 A g^{-1} (Figure S15, Supporting Information), strongly supporting that defects degrade the cathode performance (Table S2, Supporting Information). Consequently, we propose a defect-free principle for designing graphene cathode: the fewer the defects, the better the electrochemical performance. This thought is fundamentally different from previous strategies of heteroatom doping and defects introducing. Defects lead to decline of performance mainly due to three key reasons: (1) defects cannot be active sites for $AlCl_4^-$ intercalation confirmed by in situ Raman spectroscopy; (2) barricades-like defects impede the fast intercalation of $AlCl_4^-$ into graphene layers;[33] (3) defects reduce the electrical conductivity of electrode (Table S2, Supporting Information). Significantly, this defect-free principle is also valid in other AlB cases with different graphene morphologies such as nanoscrolls[44] as well as other rechargeable energy storage systems such as lithium-ion battery. The details will be reported later.

To show the comprehensive properties of Al–GB, a prototype cell was fabricated with 0.8 mg GA-3000 as cathode and Al foil as anode, sealed by cover glasses as transparent shell (**Figure 5**a,b). This Al–GB was totally charged in 36 s (a current of 100 C) with an open-circuit voltage of 2.33 V (Figure S16a, Supporting Information), which powered a red LED for 15 min (Figure 5c; Video S1 and Figure S16b,c, Supporting Information). Importantly, when the charged cell was put on the flame of an alcohol lamp (Video S2, Supporting Information), it still lighted up the red LED for 1 min without explosion (Figure 5d; Figure S16d–f, Supporting Information). Such an incomparable nonflammability of Al–GB is attributed to the incombustibility of its components especially the electrolyte. This surpasses conventional lithium batteries that need flammable and explosive organic solvents in electrolytes. Furthermore, a pouch cell was assembled with 30 mg GA-3000 as cathode, exhibiting high flexibility and twistability while lighting a LED (Figure 5e,f; Video S3, Supporting Information). The pouch cell also delivered an ultrafast charging in 2 min (≈25 C) and lighted up the LED for 2 h (Figure S16g–i, Supporting Information). Notably, it can cycle over thousands of cycles without capacity decay or any bulge due to the well-controlled cutoff voltage.[42] This combination of ultrafast charging, long-time consumption and nonflammability meets the key requirements for wearable energy storage devices, electric vehicles, and high-power electrical appliances.

In conclusion, we have proposed and demonstrated a general defect-free principle for designing advanced graphene cathode of AlB. We successfully established a highly controllable and scalable methodology with the raw material of commercially available GO and industrially viable equipments to produce GA cathode. The defect-free GA cathode affords a high specific capacity of 100 mAh g^{-1} from 2 to 50 C (average discharge voltage around 1.95 V) with unprecedent high-rate performance (97 mAh g^{-1}, 1.55 V at 500 C and 74 mAh g^{-1} at 1000 C) and excellent cycle stability (97% capacity retention after 25 000 cycles). Such record values are much higher than those of the previous Al–carbon batteries, making it the best performing cathode for AlB so far. The performances of GA cathode are highly repeatable within different batches for the defect-free design. Benefiting from the defect-free principle

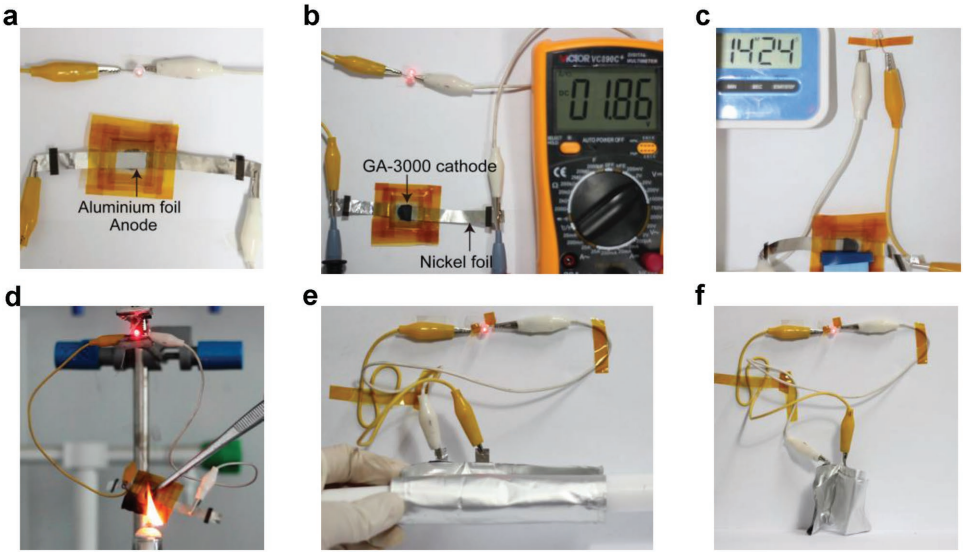

Figure 5. Exhibitions of aluminum–graphene battery (Al–GB). a) Aluminum anode and b) graphene cathode of Al–GB while c) powering a LED to test its sustainability (Video S1, Supporting Information). d) Al–GB placed in the flame of alcohol lamp while powering a LED (Video S2, Supporting Information). e) Coiled and f) folded Al–GB pouch cell while powering a LED (Video S3, Supporting Information).

(i.e., the fewer the defects, the better the performances), the Al–GB can afford an energy density of ≈60 Wh kg^{-1} comparable to commercial lead-acid batteries, a power density of ≈30 kW kg^{-1} comparable to the best graphene-based supercapacitors,[45–47] with ultralong cycling life and high safety. Such a system can be called as aluminum-graphene superbattery, and we believe that there is still plenty of room for improving the performance.[48] The first established defect-free principle would offer new sights into graphene-based electrodes of rechargeable batteries.[49]

Supporting Information

Supporting Information is available from the Wiley Online Library or from the author.

Acknowledgements

This work was supported by the National Natural Science Foundation of China (Grant Nos. 21325417, 51603183, and 51533008) and MOST National Key Research and Development Program (Grant No. 2016YFA0200200).

Received: November 4, 2016
Revised: December 7, 2016
Published online:

[1] M. Armand, J. M. Tarascon, *Nature* **2008**, *451*, 652.
[2] P. Simon, Y. Gogotsi, *Nat. Mater.* **2008**, *7*, 845.
[3] J. B. Goodenough, A. Manthiram, *MRS Commun.* **2014**, *4*, 135.
[4] N. S. Hudak, *J. Phys. Chem. C* **2014**, *118*, 5203.
[5] J. V. Rani, V. Kanakaiah, T. Dadmal, M. S. Rao, S. Bhavanarushi, *J. Electrochem. Soc.* **2013**, *160*, A1781.
[6] N. Jayaprakash, S. K. Das, L. A. Archer, *Chem. Commun.* **2011**, *47*, 12610.
[7] S. Wang, Z. Yu, J. Tu, J. Wang, D. Tian, Y. Liu, S. Jiao, *Adv. Energy Mater.* **2016**, *6*, 1600137.
[8] G. A. Elia, K. Marquardt, K. Hoeppner, S. Fantini, R. Lin, E. Knipping, W. Peters, J.-F. Drillet, S. Passerini, R. Hahn, *Adv. Mater.* **2016**, *28*, 7564.
[9] M.-C. Lin, M. Gong, B. Lu, Y. Wu, D.-Y. Wang, M. Guan, M. Angell, C. Chen, J. Yang, B.-J. Hwang, H. Dai, *Nature* **2015**, *520*, 324.
[10] H. Sun, W. Wang, Z. Yu, Y. Yuan, S. Wang, S. Jiao, *Chem. Commun.* **2015**, *51*, 11892.
[11] Y. Wu, M. Gong, M.-C. Lin, C. Yuan, M. Angell, L. Huang, D.-Y. Wang, X. Zhang, J. Yang, B.-J. Hwang, H. Dai, *Adv. Mater.* **2016**, *28*, 9218.
[12] H. Sun, Z. Xu, C. Gao, *Adv. Mater.* **2013**, *25*, 2554.
[13] L.-C. Lin, J. C. Grossman, *Nat. Commun.* **2015**, *6*, 8335.
[14] D. A. Bandurin, I. Torre, R. K. Kumar, M. Ben Shalom, A. Tomadin, A. Principi, G. H. Auton, E. Khestanova, K. S. Novoselov, I. V. Grigorieva, L. A. Ponomarenko, A. K. Geim, M. Polini, *Science* **2016**, *351*, 1055.
[15] L. Peng, Z. Xu, Z. Liu, Y. Wei, H. Sun, Z. Li, X. Zhao, C. Gao, *Nat. Commun.* **2015**, *6*, 5716.
[16] Z. Xu, C. Gao, *Nat. Commun.* **2011**, *2*, 571.
[17] Z. Xu, C. Gao, *Acc. Chem. Res.* **2014**, *47*, 1267.
[18] Z. Li, Z. Liu, H. Sun, C. Gao, *Chem. Rev.* **2015**, *115*, 7046.
[19] G. Xin, T. Yao, H. Sun, S. M. Scott, D. Shao, G. Wang, J. Lian, *Science* **2015**, *349*, 1083.
[20] Z. Xu, Y. Liu, X. Zhao, L. Peng, H. Sun, Y. Xu, X. Ren, C. Jin, P. Xu, M. Wang, C. Gao, *Adv. Mater.* **2016**, *28*, 6449.
[21] L. Qiu, J. Z. Liu, S. L. Y. Chang, Y. Wu, D. Li, *Nat. Commun.* **2012**, *3*, 1241.
[22] H. Bai, Y. Chen, B. Delattre, A. P. Tomsia, R. O. Ritchie, *Sci. Adv.* **2015**, *1*, e1500849.
[23] I. K. Moon, J. Lee, R. S. Ruoff, H. Lee, *Nat. Commun.* **2010**, *1*, 73.
[24] Z. Liu, Z. Li, Z. Xu, Z. Xia, X. Hu, L. Kou, L. Peng, Y. Wei, C. Gao, *Chem. Mater.* **2014**, *26*, 6786.
[25] M. A. Worsley, T. T. Pham, A. Yan, S. J. Shin, J. R. Lee, M. Bagge-Hansen, W. Mickelson, A. Zettl, *ACS Nano* **2014**, *8*, 11013.
[26] Y. Sun, N. Liu, Y. Cui, *Nat. Energy* **2016**, *1*, 16071.
[27] A. Hashimoto, K. Suenaga, A. Gloter, K. Urita, S. Iijima, *Nature* **2004**, *430*, 870.
[28] S. Reich, C. Thomsen, *Phil. Trans. R. Soc. Lond. A* **2004**, *362*, 2271.
[29] D. L. Duong, G. H. Han, S. M. Lee, F. Gunes, E. S. Kim, S. T. Kim, H. Kim, Q. H. Ta, K. P. So, S. J. Yoon, *Nature* **2012**, *490*, 235.
[30] L. Gao, G. X. Ni, Y. Liu, B. Liu, A. H. C. Neto, K. P. Loh, *Nature* **2014**, *505*, 190.
[31] G. Y. Yang, L. Chen, P. Jiang, Z. Y. Guo, W. Wang, Z. P. Liu, *RSC Adv.* **2016**, *6*, 47655.
[32] A. C. Ferrari, J. C. Meyer, V. Scardaci, C. Casiraghi, M. Lazzeri, F. Mauri, S. Piscanec, D. Jiang, K. S. Novoselov, S. Roth, *Phys. Rev. Lett.* **2006**, *97*, 13831.
[33] M. S. Wu, B. Xu, L. Q. Chen, C. Y. Ouyang, *Electrochim. Acta* **2016**, *195*, 158.
[34] X. Wang, G. Sun, P. Routh, D.-H. Kim, W. Huang, P. Chen, *Chem. Soc. Rev.* **2014**, *43*, 7067.
[35] J. Song, Z. Yu, M. L. Gordin, D. Wang, *Nano Lett.* **2016**, *16*, 864.
[36] Y. Liu, Z. Xu, J. Zhan, P. Li, C. Gao, *Adv. Mater.* **2016**, *28*, 7941.
[37] S. C. Jung, Y.-J. Kang, D.-J. Yoo, J. W. Choi, Y.-K. Han, *J. Phys. Chem. C* **2016**, *120*, 13384.
[38] D. Zhan, L. Sun, Z. H. Ni, L. Liu, X. F. Fan, Y. Wang, T. Yu, Y. M. Lam, W. Huang, Z. X. Shen, *Adv. Funct. Mater.* **2010**, *20*, 3504.
[39] L. J. Hardwick, M. Hahn, P. Ruch, M. Holzapfel, W. Scheifele, H. Buqa, F. Krumeich, P. Novák, R. Kötz, *Electrochim. Acta* **2006**, *52*, 675.
[40] W. Zhao, P. H. Tan, J. Liu, A. C. Ferrari, *J. Am. Chem. Soc.* **2011**, *133*, 5941.
[41] H. Meng, X. Pang, Z. Zhen, *J. Power Sources* **2013**, *237*, 229.
[42] H. Wang, S. Gu, Y. Bai, S. Chen, N. Zhu, C. Wu, F. Wu, *J. Mater. Chem. A* **2015**, *3*, 22677.
[43] J. Kotakoski, A. V. Krasheninnikov, U. Kaiser, J. C. Meyer, *Phys. Rev. Lett.* **2011**, *106*, 105505.
[44] Z. Xu, B. Zheng, J. Chen, C. Gao, *Chem. Mater.* **2014**, *26*, 6811.
[45] X. Yang, C. Cheng, Y. Wang, L. Qiu, D. Li, *Science* **2013**, *341*, 534.
[46] Y. Zhu, S. Murali, M. D. Stoller, K. J. Ganesh, W. Cai, P. J. Ferreira, A. Pirkle, R. M. Wallace, K. A. Cychosz, M. Thommes, D. Su, E. A. Stach, R. S. Ruoff, *Science* **2011**, *332*, 1537.
[47] T. Lin, I.-W. Chen, F. Liu, C. Yang, H. Bi, F. Xu, F. Huang, *Science* **2015**, *350*, 1508.
[48] S. Lee, J. Cho, *Angew. Chem. Int. Ed.* **2015**, *54*, 9452.
[49] Y. Li, K. Yan, H.-W. Lee, Z. Lu, N. Liu, Y. Cui, *Nat. Energy* **2016**, *1*, 15029.